Aerosol Science and Technology
Publication details, including instructions for authors and subscription information:
http://www.informaworld.com/smpp/title~content=t713656376

Single Particle Laser Mass Spectrometry Applied to Differential Ice Nucleation Experiments at the AIDA Chamber

Stéphane J. Gallavardin [a]; Karl D. Froyd [bc]; Ulrike Lohmann [a]; Ottmar Moehler [d]; Daniel M. Murphy [b]; Daniel J. Cziczo [e]
[a] Institute for Atmospheric and Climate Science, ETH Zurich, Zurich, Switzerland [b] Chemical Sciences Division, National Oceanic and Atmospheric Administration, Boulder, Colorado, USA [c] Cooperative Institute for Research in Environmental Sciences, University of Colorado, Boulder, Colorado, USA [d] Forschungszentrum Karlsruhe, Institute for Meteorology & Climate Research, Karlsruhe, Germany [e] Pacific Northwest National Laboratory, Atmospheric Science and Global Change Division, Richland, Washington, USA

First Published on: 01 September 2008

To cite this Article Gallavardin, Stéphane J., Froyd, Karl D., Lohmann, Ulrike, Moehler, Ottmar, Murphy, Daniel M. and Cziczo, Daniel J.(2008)'Single Particle Laser Mass Spectrometry Applied to Differential Ice Nucleation Experiments at the AIDA Chamber',Aerosol Science and Technology,42:9,773 — 791

To link to this Article: DOI: 10.1080/02786820802339538

URL: http://dx.doi.org/10.1080/02786820802339538

Aerosol Science and Technology, 42:773–791, 2008

ISSN: 0278-6826 print / 1521-7388 online
DOI: 10.1080/02786820802339538

Single Particle Laser Mass Spectrometry Applied to Differential Ice Nucleation Experiments at the AIDA Chamber

Stéphane J. Gallavardin,[1] Karl D. Froyd,[2,3] Ulrike Lohmann,[1] Ottmar Moehler,[4] Daniel M. Murphy,[2] and Daniel J. Cziczo[1,5]

[1]*Institute for Atmospheric and Climate Science, ETH Zurich, Zurich, Switzerland*
[2]*Chemical Sciences Division, National Oceanic and Atmospheric Administration, Boulder, Colorado, USA*
[3]*Cooperative Institute for Research in Environmental Sciences, University of Colorado, Boulder, Colorado, USA*
[4]*Forschungszentrum Karlsruhe, Institute for Meteorology & Climate Research, Karlsruhe, Germany*
[5]*Pacific Northwest National Laboratory, Atmospheric Science and Global Change Division, Richland, Washington, USA*

Experiments conducted at the Aerosol Interactions and Dynamics in the Atmosphere (AIDA) chamber located in Karlsruhe, Germany permit investigation of particle properties that affect the nucleation of ice at temperature and water vapor conditions relevant to cloud microphysics and climate issues. Ice clouds were generated by heterogeneous nucleation of Arizona test dust (ATD), illite, and hematite and homogeneous nucleation of sulfuric acid. Ice crystals formed in the chamber were inertially separated from unactivated, or "interstitial" aerosol particles with a pumped counterflow virtual impactor (PCVI), then evaporated. The ice residue (i.e., the aerosol which initiated ice nucleation plus any material which was scavenged from the gas- and/or particle-phase), was chemically characterized at the single particle level using a laser ionization mass spectrometer. In this manner the species that first nucleated ice could be identified out of a mixed aerosol population in the chamber. Bare mineral dust particles were more effective ice nuclei (IN) than similar particles with a coating. Metallic particles from contamination in the chamber initiated ice nucleation before other species but there were few enough that they did not compromise the experiments. Nitrate, sulfate, and organics were often detected on particles and ice residue, evidently from scavenging of trace gas-phase species in the chamber. Hematite was a more effective ice nucleus than illite. Ice residue was frequently larger than unactivated test aerosol due to the formation of aggregates due to scavenging, condensation of contaminant gases, and the predominance of larger aerosol in nucleation.

Received 5 December 2008; accepted 11 July 2008.

Funding of this work was provided by ACCENT, ETH Zürich, NOAA base funding, PECASE, PNNL LDRD, and the European Union Integrated Project SCOUT-O3. We wish to thank the AIDA team, the IN08 participants, and David Thomson for their assistance in preparing these experiments. We also thank Joseph Ulanowski for providing SID-2 data.

Address correspondence to Daniel Cziczo, Pacific Northwest National Laboratory, Atmospheric Science and Global Change Division, P.O. Box 999, Richland, WA 99352, USA. E-mail: daniel.cziczo@pnl.gov

INTRODUCTION

One of the largest uncertainties associated with our current understanding of climate is the relationship between aerosol particles and cloud formation (Forster et al. 2007). Commonly termed the indirect effect, it is known that changes in aerosol properties can result in changes in clouds which, in turn, affect the Earth's radiative balance. It is believed that the net indirect effect acts opposite that of greenhouse gas warming but the magnitude is poorly constrained (Forster et al. 2007). The indirect effect can be subdivided into specific changes in aerosol properties and some of these are relatively well understood. For example, it has been shown that an increase in aerosol number density will increase the number of cloud droplets while simultaneously reducing their size. This results in a longer cloud lifetime, a higher albedo, and a reduction of precipitation (Twomey 1974).

Glaciation, that is the initiation of the ice phase within clouds, is less well understood. Ubiquitous sub-micrometer atmospheric aerosols, most often composed of aqueous mixtures of salts and organics, typically only experience spontaneous formation of ice, termed homogeneous freezing, at temperatures below -36°C and saturations near that of liquid water (DeMott 2002). It has been known for some time that certain materials induce the freezing process at much higher temperatures and lower saturations via a heterogeneous pathway (Pruppacher and Klett 1997). These materials, termed ice nuclei, are normally insoluble and refractory, such as mineral dusts and metal oxides (Pruppacher

and Klett 1997). More recently it has been shown that effloresced soluble material, specifically ammonium sulfate and oxalic acid, can act in the same manner (Abbatt et al. 2006; Zobrist et al. 2005).

Not all IN induce ice nucleation at precisely the same temperature and saturation, however. Part of this is due to the different "modes" by which heterogeneous ice nucleation can take place. At low saturation water vapor may deposit directly to the ice nucleus (deposition mode) whereas at higher saturation an IN can induce ice nucleation from within a water capsule (immersion mode; Vali et al. 1978). A less well studied process is that of ice formation due to an ice nucleus coming in contact with a droplet or aqueous particle (contact mode; Cantrell and Heymsfield 2005). Different ice nuclei exhibit different required conditions to induce ice nucleation in the same mode and the same type of ice nucleus often exhibits different ice formation properties across the modes (Pruppacher and Klett 1997). The presence of atmospherically relevant surface coatings (e.g., organics and sulfates) generally "deactivate" (i.e., reduce the required temperature and/or increase the saturation) the ice nucleation potential of an IN in deposition mode (Georgii 1963; Braham and Spyers-Duran 1974; Pruppacher and Klett 1997 and references therein). Complicating the issue further, different experiments have shown very different ice nucleation requirements for what appear to be the same type of particles. One atmospherically important species for which there is a lack of consensus on the point at which freezing begins is black carbon (DeMott 1990; Diehl and Mitra 1998; DeMott et al. 1999; Gorbunov et al. 2001; Möhler et al. 2005; Dymarska et al. 2006).

These results illustrate the need for more, and more comprehensive, studies of ice nucleation if we are to better understand the indirect effect due to glaciation on the Earth's radiative budget. Towards this goal we describe here studies of ice nucleation within the AIDA chamber (Möhler et al. 2006) during which a single particle aerosol mass spectrometer was deployed. Experiments presented in this paper were conducted with external mixtures of heterogeneous ice nuclei such as Arizona test dust, illite, and hematite. Sulfuric acid, a particle type that can only undergo homogenous freezing, was used for comparison. Ice crystals nucleated in the AIDA chamber were inertially separated from the unactivated aerosols using a PCVI (Boulter et al. 2006). Chemical composition and size was determined by melting and evaporating the condensed-phase water and analyzing the residual material with the Particle Analysis by Laser Mass Spectrometry (PALMS) instrument (Cziczo et al. 2003; Cziczo et al. 2006). Simultaneous measurements using complementary AIDA facility instruments are also presented for comparison.

This technique is shown to be an additional tool for ongoing efforts to better understand ice nucleation. The capability to determine composition on a particle-by-particle basis allows for differentiation where aerosol size, shape, and density are similar. The detection limits of single particle mass spectrometry allow for characterization of thin surface coatings and/or the occurrence of trace constituents which are undetectable in traditional instruments used at the AIDA chamber. Finally, the sensitivity of this technique allowed for the detection of scavenging processes within the AIDA chamber which previously had not been characterized but which may affect data interpretation.

METHODOLOGY

The AIDA Chamber

To investigate ice nucleation of various aerosols the AIDA facility was operated as a dynamic cloud expansion chamber as described in detail by Möhler et al. (2005a, 2006). The aerosol vessel of 84 m^3 volume is located in a thermally insulated housing (Figure 1) which can homogeneously be cooled to low temperatures. The experiments described here, termed the IN08 campaign, were conducted during fall 2005. Cloud expansion runs are started at a pre-selected constant temperature, either about 254 K or 244 K for these experiments, atmospheric pressure (about 1000 hPa), and almost ice saturated conditions maintained by a thin ice coating on the walls inside the aerosol vessel. A mixing fan was used to keep the temporal and spatial temperature variability in the vessel within $\pm 0.3^{\circ}$C.

Ice supersaturated conditions are achieved by pumping from $\sim$1000 hPa to $\sim$800 hPa within a few minutes. A typical data set of an AIDA expansion run is shown in Figure 2 for experiment IN08-34. The wall temperature T_w remains almost constant

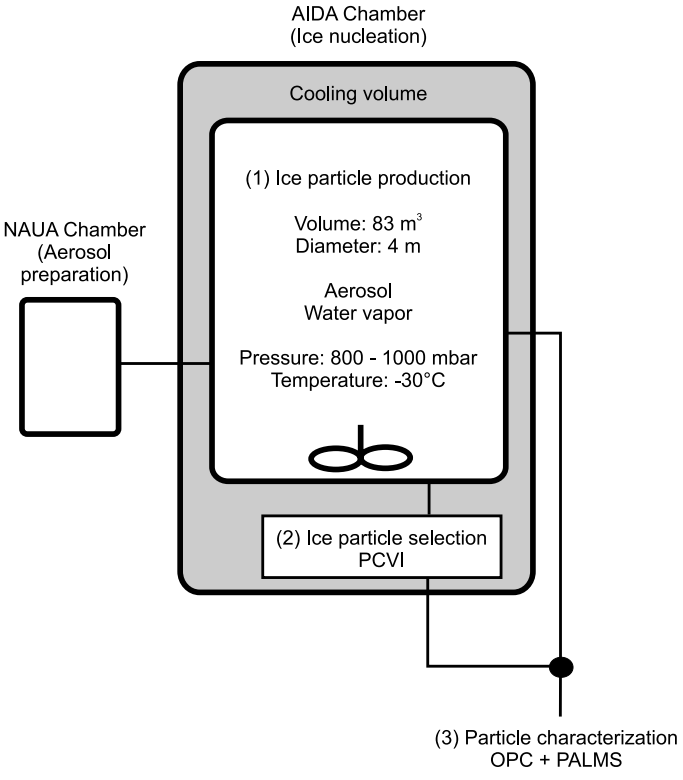

FIG. 1. Overview of the experimental setup. For a complete description of the technical characteristics of the AIDA chamber and the remainder of the available instrumentation refer to Möhler et al. (2006).

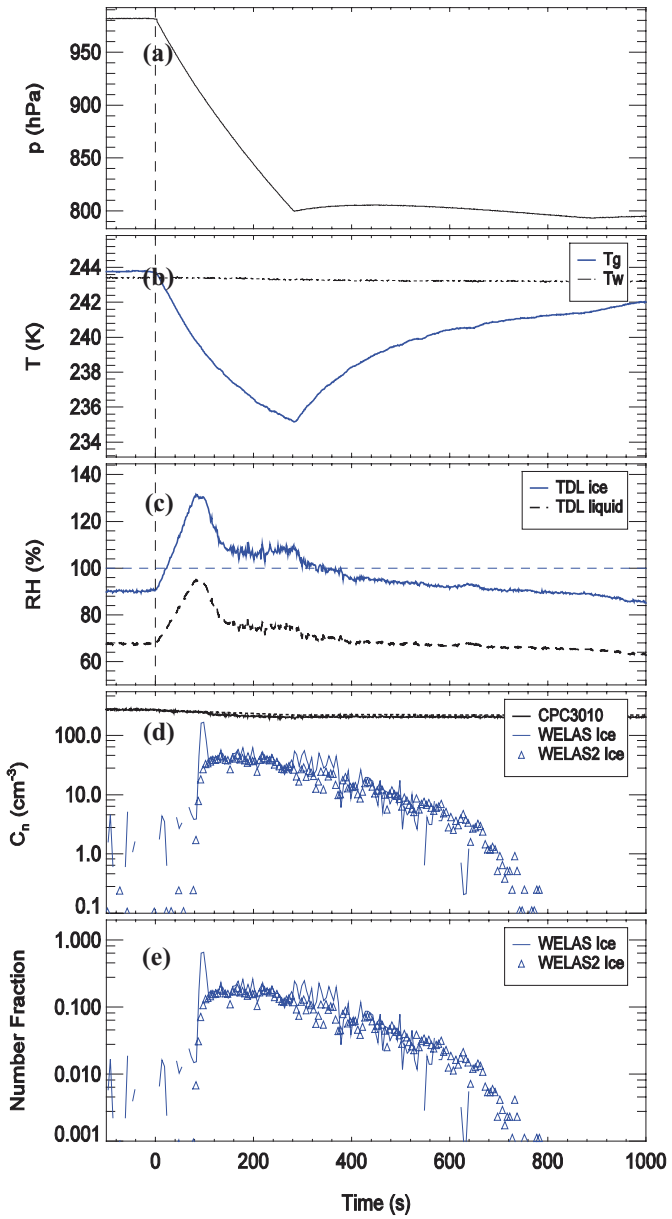

FIG. 2. Time series of AIDA gas pressure (a), mean wall temperature T_w and gas temperature T_g (b), relative humidity (c), solid blue line with respect to ice, dashed black line with respect to water), aerosol and ice particle number concentrations (d), and fraction of ice particle to aerosol particle number concentration (e). The aerosol number concentration (black line of panel d) was measured with a condensation particle counter (CPC3010), the ice number concentrations and fractions of panels (d) and (e), respectively, were measured with two optical particle counters (WELAS and WELAS2, blue lines and triangles, respectively). Data shown are for experiment IN08-34.

(panel a), whereas the gas temperature T_g (panel b) is lowered during pumping expansion (panel a), and starts to rise again after pumping stops due to heat fluxes from the warmer vessel walls. The relative humidity with respect to ice RH_i (panel c) is calculated from the actual water vapor partial pressure, measured with a tunable diode laser instrument (Möhler et al. 2006), and the ice saturation pressure at T_g (Murphy and Koop 2005). The aerosol number concentration n_{ae} (black line in panel d) is measured with a condensation particle counter (TSI Inc., type CPC3010) directly sampling from the aerosol vessel through a horizontal tube. Two optical particle counters (Fa. Palas, Welas type) are connected to vertical sampling tubes below the aerosol vessel and measure the ice particle number concentration concentrations n_{ice} (blue lines and triangles in panel d). The ice active fraction f_{ice} of the aerosol particles (panel e) is calculated as the ratio of n_{ice} to the total particle concentration.

The ice-active fraction is a direct measure for the ice nucleation efficiency of the aerosol added to the AIDA vessel. If expansion runs with different aerosols are compared for the same starting temperature and rates of pressure, temperature, and humidity change, more active heterogeneous ice nuclei show earlier ice formation onset, i.e., at warmer temperatures and lower supersaturations, and larger ice-active particle fractions f_{ice} (Möhler et al. 2006). The cooling rates applied during the expansion runs discussed in the present work mimic that of atmospheric air parcels ascending with a vertical velocity of about 0.1 to 2 m/s. One of the advantages of the AIDA facility is that ice nucleation processes can be studied at conditions which are similar to those of ascending air parcels in lee wave or convective clouds.

Ice nucleation within the AIDA chamber can be due to several of the mechanisms described in the introduction. Deposition nucleation is the probable mechanism below water saturation and for particles that do not readily activate as droplets. For conditions above water saturation and when droplets are present immersion freezing can also take place. For those experiments with aqueous particles and when the temperature drops below −36°C homogeneous freezing is also possible.

Pumped Counterflow Virtual Impaction

A PCVI separates a particle population into two size fractions. Vacuum pumping draws particle-laden air into the PCVI inlet, which then passes through a short constriction to accelerate the flow. A counterflow of particle-free air creates a stagnation region in the middle of the PCVI, which inertially separates particles. Particles with high inertia pass through the stagnation region and are sent to monitoring instruments. Low inertia particles are caught in the counterflow and are removed by the main pump flow. Counterflow virtual impactors are characterized by a 50% cutpoint: the diameter where half the particles are transmitted. Under non-turbulent operating conditions the PCVI cutpoint increases with the pressure in the stagnation region (Boulter et al. 2006).

Two PCVIs, one from NOAA and the second from AIDA, which operated under slightly different conditions were employed in this study. The inlet-to-collection orifice distance was 2.2 mm (NOAA) and 1.6 mm (AIDA). The AIDA model had a 1.4 mm diameter inlet constriction, whereas the NOAA model used a smaller 1.0 mm constriction. As a result, to reject

unactivated aerosol the NOAA PCVI generally required higher counterflows (6–9 vlpm) and pump flows (9–15 vlpm) than the AIDA model (1–2 and 10–12 slpm). Inlet flows were typically 4–8 vlpm (NOAA) and 8–11 slpm (AIDA), and outlet flows were 1–2 vlpm. The activated particle concentration inside the AIDA chamber can thus be calculated using PCVI flows and pressures, flows into the particle counters, and the chamber pressure.

This set of expansions marked the first time a PCVI was used for inertial separation of particles from the AIDA chamber. As such, activated particle transmission varied throughout the study as optimum flow conditions were determined. Representative transmission curves for the two PCVIs are shown in Figure 3. To estimate the PCVI transmission curve, residue concentrations measured downstream of the PCVIs were compared to activated particle concentrations measured inside the AIDA chamber over the course of the expansion. A sigmoidal function was applied to the activated particle size distribution. The sigmoidal function that resulted in the best match between the total activated aerosol concentration and the residue concentration over time is considered the PCVI transmission curve. Note that, while this is a best match, there can be multiple solutions for the sigmoidal function to the distribution. The fit is insensitive to the width of the sigmoidal function, but the 50% cutpoint is constrained to less than ± 1 μm. Size distributions of activated particles were measured using either the FTIR for liquid droplets (expansion IN08-20) or the SID-2 instrument for ice crystals (IN08-13). Cutpoints were typically 4–7 μm diameter so that activated particles were efficiently separated from unactivated aerosol. Transmission efficiency decreased for ice crystals larger than about 20 μm.

At the beginning of the expansion, flows were adjusted to fix the PCVI pressure to chamber pressure minus 60 mbar (AIDA) or 850–950 mbar (NOAA). The pump flow and counterflow for the AIDA PCVI were kept at a constant mass flow (increasing volumetric flow) during the expansion. The NOAA PCVI pump and outlet flows were regulated by throttled valves to mechanical pumps, and all volumetric flows decreased during the expansion. The NOAA counterflow had to be periodically adjusted to prevent transmission of interstitial aerosol. The PCVI pressure for both models decreased during the expansion, bringing the cutpoint down to as low as ~ 2 μm (Boulter et al. 2006) while still maintaining efficient separation of ice crystals and interstitial aerosol. Thus, during some time periods un-activated particles were transmitted through the PCVI as the flows were changed. These particles were removed from the data set and specifics conditions and fractions are given in the description of the relevant experiments. The PCVIs were mounted directly to the bottom of the AIDA chamber inside the cooling volume so that ice crystals were not heated during separation. From each PCVI, transmitted ice crystals traveled 3.5 m inside a 7 mm i.d. tube before exiting the chamber cooling volume, then through a short section heated to 40°C to evaporate the ice. Ice residue was sampled by the PALMS, OPC, and CPC instruments (see next sections).

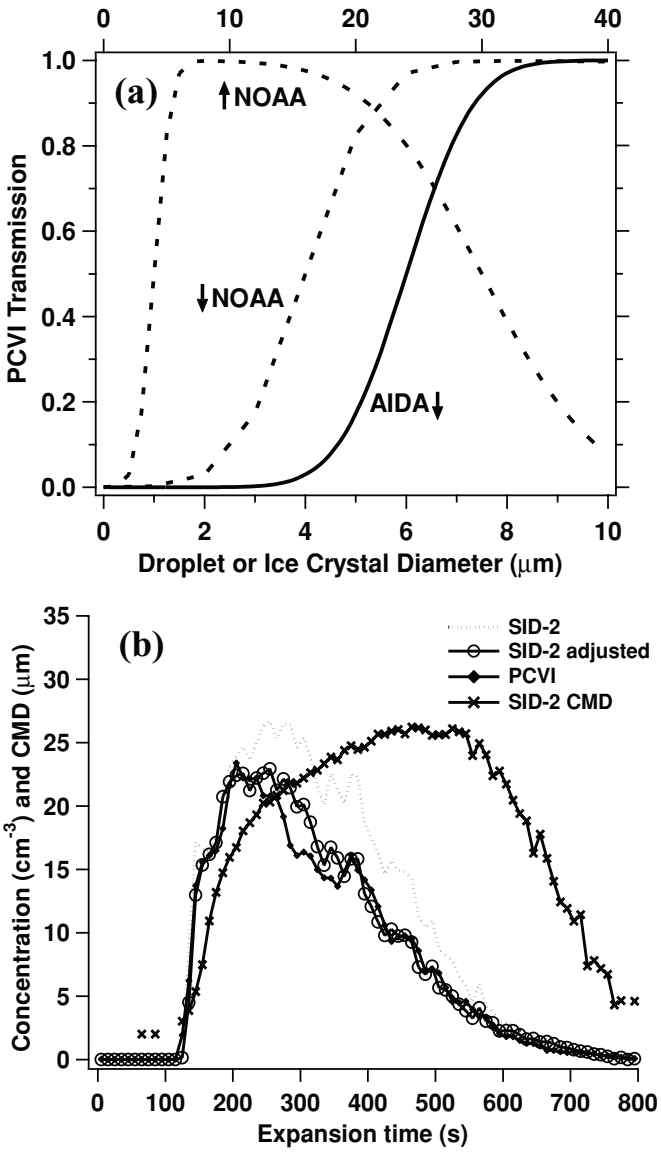

FIG. 3. Transmission efficiency for the PCVIs (a). AIDA curve (solid) is calculated for IN08-20, and NOAA curve (dashed) is for expansion IN08-13. The same NOAA curve is also plotted on an expanded scale (top axis) to show transmission drop-off at large sizes. In (b) SID-2 total ice particle concentrations and count median diameters are plotted over time for IN08-13. Applying the NOAA PCVI transmission curve in (a) to the SID-2 size distributions (not shown) at every time point in (b) gives the adjusted SID-2 total concentration curve.

Prior to expansion experiments, standard glass particles (Merck, Darmstadt, Germany) were injected into the PCVI for calibration and testing. Glass particles were occasionally observed when sampling through the PCVI during expansion experiments, although they were never observed during pre- or post-expansion sampling. Presumably, glass particles that were stuck to the tubing and PCVI walls were dislodged by large ice crystals. These contaminants were removed from PALMS spectra and OPC size distributions.

PALMS

After heating, ice residue from the PCVI was conducted via steel tubing and silicon conductive tubing to the inlet of the PALMS instrument. The combination of the dry counterflow air, heating of the sample flow behind the PCVI, and the laboratory temperature outside the AIDA chamber caused evaporation of the condensed-phase water of the ice crystals. PALMS then allowed for the characterization of the size and chemical composition of the ice residue at the single particle level. The configuration of the PALMS instrument for ice nucleation studies has been recently described by Cziczo et al. (2006). Briefly, the PALMS instrument focuses 200 nm–3 μm particles with an aerodynamic lens. Once in the vacuum chamber, particles are detected as they successively scatter the light from YAG timing and detection laser beams (532 nm, continuous wave, 25 mW each). The particle trajectory results in approximately one in ten particles scattering light from the detection beam sufficient to be detected by a photomultiplier. Depending on composition, approximately 90% of these particles also scatter sufficient light from the timing beam. The time between light scattering events allows the particle velocity to be measured and from this the particle vacuum aerodynamic size can be inferred (Wilson and Liu 1980; Prather et al. 1994). The magnitude of the scattered light from either beam can also be correlated to particle geometric size. The particle density can then be inferred by combining the vacuum aerodynamic diameter with the magnitude of the scattered light (Murphy et al. 2004; Moffet and Prather 2005; Cross et al. 2007). Each light scattering event from the detection laser triggers an excimer laser (193 nm, $\sim$4 mJ per pulse) that desorbs and ionizes the particle components. The ions are analyzed by time-of-flight mass spectrometry at either positive or negative polarity, thus providing compositional information for that single particle. The PALMS hardware and software operate sufficiently fast to record particle size and mass spectra at a rate of up to 7 Hz.

OPC and CPC

To supplement the PALMS counting and sizing capabilities a white light particle counter (Climet 208 outfitted with a multichannel analyzer) and condensation particle counter (TSI model CPC3010) were mounted in parallel. The two utilized CPC3010 instruments, one connected to the AIDA PCVI and the other directly sampling from the AIDA aerosol vessel, were modified and calibrated for reduced pressure sampling (Seifert et al. 2004). The OPC monitored aerosol size distributions from 0.3 to $\sim$6 μm diameter, but counting efficiency decreased below $\sim$0.4 μm. The OPC was calibrated using polystyrene latex spheres (Duke Scientific, Fremont, CA, USA). Mie scattering calculations were performed to convert raw diameters to equivalent sphere diameters for sulfuric acid, mineral dust, and hematite. Densities and indexes of refraction were 1.05 g cm^{-3} and 1.59 for latex spheres, 1.7 g cm^{-3} and 1.4 for sulfuric acid aerosol, 2.6 g cm^{-3} and 1.5 for mineral dust, and 5.3 g cm^{-3}and 2.94 for hematite. All aerosol types were assumed to be nonabsorbing. For most experiments the aerosol size distribution extended below the lower size limit of the OPC. Therefore, total residue concentration measurements reported here are multiplied by a scaling factor (typically $\sim$1.5–3) that was determined by comparing the OPC and CPC concentrations prior to each expansion. A constant scaling factor was used for each experiment, although the scaling factor may have increased slightly over the course of some expansions. Additionally, all OPC and CPC total residue concentrations are multiplied by a factor of 2.0 to help account for particle loss to the PCVI and tubing walls. This factor is based on previously observed losses in the PCVI (Boulter et al. 2006) and to the tubing between the AIDA chamber and the analytical instruments. This factor is used to facilitate comparisons with other techniques, not to draw conclusions regarding absolute concentrations. The OPC drew 0.5–1.0 vlpm from PCVI outlet line in parallel to PALMS. There was no observable change in counting efficiency over the range of experimental flows and pressures.

Test Aerosols

We present experiments conducted during the AIDA ice nucleation campaign IN08 with Arizona test dust, hematite, illite, and sulfuric acid. ATD and sulfuric acid aerosols were chosen because their ice nucleation ability has already been investigated at the AIDA and other chambers (Möhler et al. 2003; Möhler et al. 2005; Archuleta et al. 2005; Möhler et al. 2006). ATD is known to be an effective heterogeneous ice nucleus whereas sulfuric acid only freezes homogeneously (i.e., at higher ice supersaturation and temperatures only below -36°C). An external mixture of hematite and illite was chosen because these particles are chemically distinct and thus can be differentiated with PALMS. Since both particle size distributions were similar it would not be possible to differentiate them with the current AIDA facility instruments, however. Hematite was synthesized at the AIDA facility. The illite and ATD samples were obtained from B+M Nottenkämper (Munich, Germany) and PTI Powder Technology, Inc. (Burnsville, MN, USA), respectively. The mineral particle samples were directly dispersed into a flow of particle-free (<0.001 particles per cubic centimeter) dry synthetic air either with a rotating brush generator (RBG1000, Fa. Palas) or a small scale powder disperser (SSPD, TSI Inc.). The synthetic air originated from compressed gas cylinders with less than 3 part per million (ppm) water vapor and less than 0.5 ppm hydrocarbon content Larger dust particles were removed in an inertial impactor with a cutoff diameter of about 1 μm before the aerosol was added to the aerosol chamber. The sulfuric acid particles were generated by first saturating a 2 l/min flow of synthetic air with sulfuric acid at about 140°C. Sulfuric acid/water droplets nucleated upon cooling of the saturated mixture and were directly added to the cloud chamber through a Teflon tube.

TABLE 1
Experimental conditions

Experiment	Aerosol System	Size & Concentration	PALMS PCVI	Day	Start Time	T_0 (K)
IN08-19	AIDA chamber background	Background particles: 0.25/cm^3	NOAA	21.11.05	9:52	243.6
IN08-20	SA	SA: mode 600 nm 33/cm^3	NOAA	21.11.05	12:15	243.6
IN08-21	SA	SA: mode 600 nm 28/cm^3	AIDA	21.11.05	14:00	243.7
IN08-22	SA + ATD (ext.)	SA: mode 600 nm ATD: mode 600 nm 38/cm^3	NOAA	21.11.05	17:00	243.8
IN08-23	ATD	ATD: mode 450 nm 300/cm^3	NOAA	22.11.05	10:35	253.8
IN08-24	ATD	ATD: mode 450 nm 210/cm^3	AIDA	22.11.05	13:25	253.9
IN08-25	ATD + SA (ext.)	ATD: mode 450 nm SA: mode 600 nm Total: 300/cm^3	NOAA	22.11.05	17:20	253.7
IN08-32	Hematite	Hematite: mode 500 nm$^{(m)}$ 305/cm^3	NOAA	25.11.05	10:40	243.6
IN08-33	Hematite + Illite (ext.)	Hematite: mode 500 nm$^{(m)}$ Illite: mode 500 nm Total: 400/cm^3	NOAA	25.11.05	14:00	243.7
IN08-34	Hematite + Illite (ext.)	Hematite: mode 500 nm$^{(m)}$ Illite: mode 500 nm Total: 270/cm^3	NOAA	25.11.05	16:00	243.8

T_0: Temperature in the chamber before the expansion starts, SA: Sulfuric acid, ATD: Arizona Test Dust, ext.: external mixture, $^{(m)}$ monodisperse particles.

Data Analysis

Three expansion experiments were conducted during a typical day during IN08 of which normally two were on the same test aerosol with the third on a different system. Specific conditions of each expansion presented here are given in Table 1. For the PALMS data analysis and evaluation, each experiment was separated into a pre-expansion, an expansion, and a post-expansion phase referred to in the text and figures as Pre-Exp, Exp (i, ii, iii, etc.) and Post-Exp, respectively. These studies were focused on the composition of ice residue during the expansion phase and the total aerosol during the pre- and post-expansion phases. Several hundred particles were analyzed in both ion polarities during the pre- and post-expansion phases in order to characterize the aerosol before and after the ice nucleation event. During the expansion phase the polarity of PALMS was changed once or twice during the several-minute period during which ice crystals were present. This was done because different polarity mass spectra provide complementary information. Positive mass spectra resolve trends in metallic ions (e.g., iron, rubidium, strontium, barium) whereas negative polarity allows for monitoring of sulfate, nitrate, and aluminosilicate ions, among others. The number of changes was limited since a switch of PALMS polarity requires ~15 seconds. Mass spectra acquired during the expansion phase were further grouped into subsets in order to follow the ice residue particle size and composition change as a function of the different temperature and supersaturation conditions in the AIDA chamber. Thus, lower case roman numerals (e.g., i, ii, iii, etc.) are used to denote successive periods within the expansion phase based on a change in polarity and/or a change in experimental conditions (e.g., the onset of homogeneous ice nucleation during experiments where the expansion led to temperature below −36°C). Table 2 summarizes the number of particles analyzed by the PALMS instrument during the experiments.

The chemically distinct nature of the test aerosols allowed for simple mass spectral separation based on the presence or absence of ions. The presence of ions from multiple particle types in one mass spectrum was inferred to be the result of particle-phase scavenging by ice during expansions or agglomeration between expansions. The presence of both principle (Al, Si, Fe, etc.) and trace species (e.g., Rb, Sr, Ba, and Cl) was also monitored.

The presence of other species, namely sulfates, nitrates, and organics, was also monitored since it is known that surface coatings or surface chemistry can reduce the ice nucleating potential of dust particles (Pruppacher and Klett 1997). Some of the experiments performed during IN08, not all of which are described here, included external mixtures of mineral dust particles and sulfuric acid droplets. As discussed more fully in subsequent sections, materials such as sulfates, nitrates, and organics were found mixed with other particles even during periods when they were not intentionally added to the AIDA chamber. During these times their presence is attributed to gas-phase scavenging of material remaining from past expansions and/or trace components of the dispersed dust samples.

Finally, particle size was monitored throughout the course of an experiment. Previous work indicates the dependence of the heterogeneous ice nucleation activity of dust particles on their

TABLE 2

Polarity (top row), total number of mass spectra acquired during each experimental phase (middle row), and number of mass spectra that lead to the particle's composition identification (bottom row). Both polarities were sampled during Pre-Exp and Post-Exp phases. Depending on time, from one to two sets of data at alternating polarity were acquired during an expansion. Each expansion is further subdivided (labeled i to vi) in order to follow the composition of the ice residue as a function of time (i.e, water saturation)

Experiment	Pre–Exp	Exp(i)	Exp(ii)	Exp(iii)	Exp(iv)	Exp(v)	Exp(vi)	Post-Exp
IN08-01								
Polarity	(+)							
Number	326							
Identified	160							
IN08-19								
Polarity	(+)	(+)						(+)
Number	80	70						36
Identified	35	47						5
IN08-20								
Polarity	(+) – (−)	(−)*	(−)	(−)	(−)	(−)	(−)	(+) – (−)
Number	833– 744	7	83	134	826	845	1172	298–370
Identified	635–606	1	70	79	445	443	621	178–279
IN08-21								
Polarity	(+) – (−)	(−)*	(−)	(−)	(−)	(−)		(+) – (−)
Number	319–582	4	528	160	100	124		281–205
Identified	205–426	1	375	95	51	72		142–164
IN08-23								
Polarity	(+) – (−)	(+)*	(+)	(+)	(−)	(−)		(+) – (−)
Number	712–765	8	374	361	733	853		495–488
Identified	193–314	2	119	103	189	166		120–148
IN08-24								
Polarity	(+) – (−)	(+)*	(+)	(+)	(+)	(+)	(−)	(+) – (−)
Number	798–815	5	159	148	103	39	44	401–308
Identified	215–314	5	145	130	91	33	23	202–279
IN08-33								
Polarity	(+) – (−)	(+)	(+)	(+)	(+)	(+)	(+)	(+) – (−)
Number	553–559	32	35	486	430	549	446	769–896
Identified	313–517	26	34	451	417	537	426	566–840
IN08-34								
Polarity	(+) – (−)	(+)	(+)	(+)	(−)	(−)		(+) – (−)
Number	931–673	48	1037	531	518	624		743–649
Identified	663–612	43	942	509	409	442		553–601

Pre-Exp and Post-Exp denote measurements performed before the beginning of the expansion and after the ice cloud had dissipated, respectively.

Note that experiment IN08-01 was a characterization of the background aerosol in the AIDA chamber and did not include an expansion. IN08-19 was an expansion with only the background aerosols. Expansion periods marked with an asterisk (*) are not included in the analysis due to the limited number of spectra.

diameter or surface area (e.g., Archuleta et al. 2005). The height of the detection beam light scattering peak, which is correlated with geometric area, was monitored (Murphy et al. 2004). Although less sensitive to size than the vacuum aerodynamic diameter derived from the dual timing beams, this method was preferred because it is known that pressure changes at the inlet of an aerodynamic lens can change the focus as a function of particle size (Zhang et al. 2004; Liu et al. 2007) and terminal velocity (Zhang et al. 2004). Rapid pressure changes (from 1000 down to 800 mbar) were an inherent part of each expansion phase.

The specific ions attributed to each test aerosol type are listed in Table 3. In negative polarity hematite was identified by the series of iron oxide ions Fe_xO_y (Figure 4a) and in positive polarity by the isotopic ions of iron (Figure 4b). The presence of Cl^- ($m/z = 35, 37$) is a by-product of hematite synthesis.

TABLE 3
Particle class, abbreviation used in the figures, polarity, and mass spectral components

Particle Class	Abbreviation	Polarity	Components Detected in Mass Spectra
Hematite	Hematite	+	Fe only
Illite	Illite	+	K, Al, Si, Fe
Mineral Dust	MD	+	Na, K, Al, Si, Fe with or without any combination of Li, Rb, Sr, Ba
Mineral Dust -X	MD -X	+	K with any combination of Rb, Sr, Ba but without Fe, Na, Al, Si
Sulfates	Sulf.	+	Sulfates fragments: H_xSO_y
Mineral Dust + Sulfates	MD + Sulf.	+	Mineral dust particles with sulfates
Mineral Dust + Sulfates + Nitrates	MD + Sulf. + Nit.		Mineral dust particles with sulfates and nitrates
Undefined	Undefined	+	Particles not classified above
Hematite	Hematite	−	Iron oxides Fe_xO_y
Illite	Illite	−	Aluminum and/or silicon oxides $(Al,Si)_xO_y$
Hematite + Illite Aggregate	Hematite + Illite Aggregate	−	Aluminum and/or silicon oxides $(Al,Si)_xO_y$+ iron oxide ion FeO_2
Mineral dust	MD	−	Aluminum and/or silicon oxides $(Al,Si)_xO_y$
Sulfates	Sulf.	−	Sulfates fragments
Nitrates	Nit.	−	Nitrates fragments
Mineral Dust + Sulfates	MD + Sulf.	−	Mineral dust particles with sulfates
Mineral Dust + Sulfates + Nitrates	MD + Sulf. + Nit.	−	Mineral dust particles with sulfates and nitrates
Sulfates + Nitrates	Sulf. + Nit.	−	Sulfates + Nitrates
Undefined	Undefined	−	Particles not classified above

Illite presented a series of aluminum and silicon oxide ions, $(Al,Si)_xO_y$, in negative polarity (Figure 4c) while in positive polarity spectra were dominated by potassium, aluminum, silicon, and iron ions (Figure 4d). Arizona test dust is spectrally similar to illite although with different peak height ratios. Negative mass spectra (Figure 4e) exhibited ions of mass m/z = 60 (SiO_2), 76 (SiO_2.O), 120 (($SiO_2)_2$), and 136 (($SiO_2)_2$. Positive mass spectra showed the presence of sodium (Figure 4f) which was not found for illite. Trace elements such as strontium, rubidium, and barium are easily ionized and were also frequently detected in various ratios in both illite and ATD. Analyses from the manufacturer show that these elements are only present in trace amounts so these peaks are attributed to their low ionization threshold. Sulfuric acid particles were identified by the series of sulfur oxide ions H_nSO_m with m = 0 – 4 and n = 1,3 in both negative and positive polarity. Typical sulfuric acid mass spectra are shown in Figure 4g and h.

The production of ions when a particle is detected by a single particle instrument is a complex function of the location of the particle in the desorption beam, size, phase, composition, and laser power (e.g., Zelenyuk and Imre 2005). This leads to differences in the quantity of ions such that not all mass spectra have sufficient ions to be clearly identified. Table 2 indicates for each experiment the fraction of particles whose chemical composition was clearly identified. In the pre-expansion phase 55, 25, and 60% of particles from hematite-illite mixture, ATD, and sulfuric acid experiments produced a mass spectrum allowing for identification in positive polarity, respectively. In negative polarity 90, 40, and 70% of particles were identified. The remainder of mass spectra are classified here as "undefined."

Minor and trace compounds were common in both pre- and post-expansion particles and the ice residue. Nitrates were commonly found in residue spectra during the expansion phase. These species were characterized by ions at m/z = 46, 62 (NO_2^- and NO_3^-) and m/z = 30 (NO^+) in negative and positive polarity, respectively. Carbonaceous material, the presence of ions of the generic formula C_nH_m, was found for the majority of particles. A species with m/z = 42 that could be CNO^- or $C_2H_2O^-$ was frequently detected. It is labeled as m/z = 42 since its nature in these experiments could not be definitively determined.

EXPERIMENTAL RESULTS

Background Particles

Background measurements and one control experiment were conducted during IN08. Background measurement was conducted before experiment IN08-01 which consisted of sampling of the AIDA chamber after it had been evacuated and refilled with synthetic air. Since the CPC counts were non-zero during these periods, averaging 0.8 cm^{-3}, it was known that the AIDA background was not completely particle free. We thus term these "background particles." The second was experiment

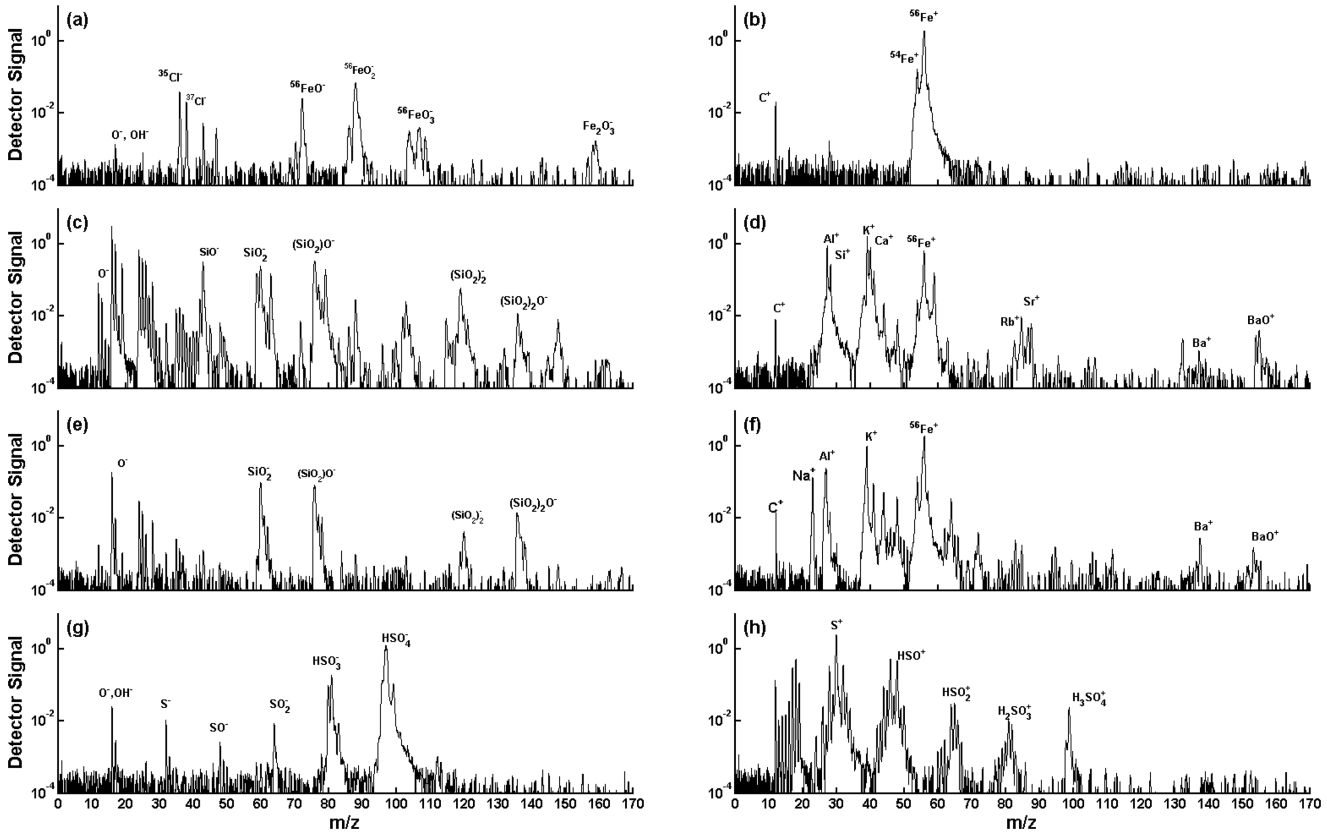

FIG. 4. Mass spectra of hematite (a), (b), illite (c), (d), ATD (e), (f), and sulfuric acid (g), (h). Left panels: typical negative mass spectra. Right panels: typical positive mass spectra. These aerosol types have different components or, in the case of illite and ATD, different component ratios, and are thus differentiable with single particle laser ablation mass spectrometry.

IN08-19, which consisted of an evacuation and refill of the chamber with only synthetic air followed by an expansion. Average CPC counts in IN08-19 were 0.3 cm^{-3} and the OPC indicated all were below 0.7 μm diameter.

PALMS spectra typical of both experiments but specific to the pre-expansion phase of IN08-19 are shown in Figure 5. Panel (a) depicts a particle spectrum with positive ions due mainly to iron, chromium, and molybdenum with less amounts of other metals. These components are consistent with stainless steel. Panel (b) depicts a particle mass spectrum of positive ions comprised almost exclusively of aluminum with lesser signals due to iron and copper. This is consistent with an aluminum alloy. It should be noted that a variable fraction of particles were below the PALMS detection limit and these may or may not follow this composition. The presence of metallic particles is not altogether surprising in that they may be present in the synthetic air system and the AIDA chamber, which is an aluminum-walled vessel that includes numerous instrument ports with stainless steel valves. This result illustrates that nominally particle-free air in these experiments is not truly devoid of particles. Reference expansions during past AIDA experiments show that most background particles only activate close to the homogeneous freezing threshold. It is known, however, that metallic particles are highly efficient ice nuclei (DeMott et al. 2003). Onset conditions in IN08-19 indicate that ice crystals begin to form for a water supersaturation ratio with respect to ice of 1.3 at an experimental temperature of –33°C. This result indicates that some

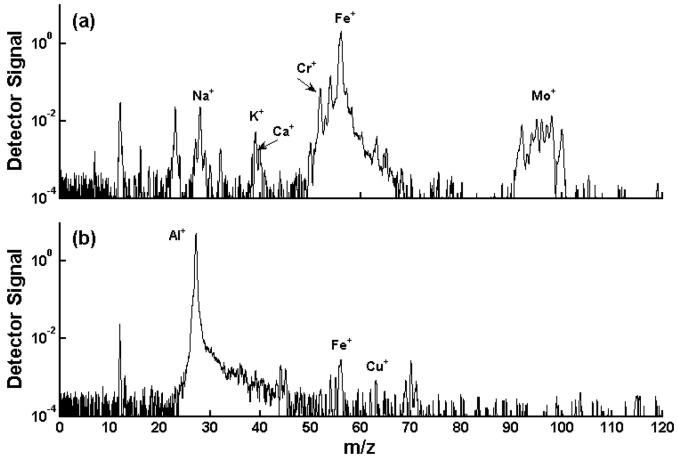

FIG. 5. Examples of "background particles" found in a nominally particle-free AIDA chamber during experiment IN08-19. Particles are consistent with stainless steel (a) and aluminum (b) and likely originated from the chamber walls and/or instrument ports.

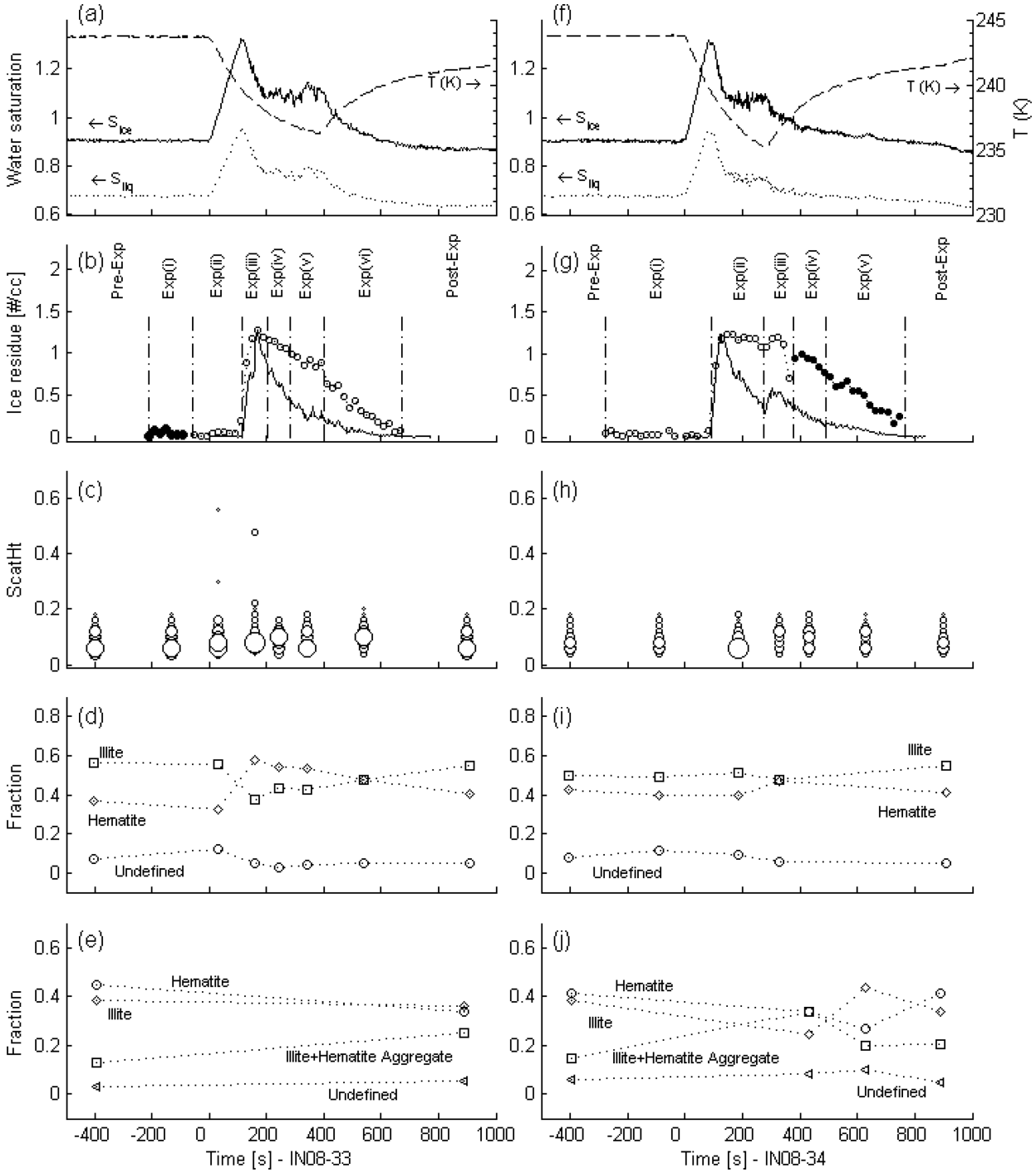

FIG. 6. Variation of the water supersaturation ratio with respect to ice, PALMS hit rate (expressed as a concentration), particle size, and composition as a function of time for experiment IN08-33 (left) and IN08-34 (right). The test aerosol was an external mixture of hematite and illite. Time t = 0 corresponds to the start of the AIDA pumps (i.e., the expansion phase). Pre-Exp, Exp(i, ii, iii, iv, v, vi), and Post-Exp are as defined in Table 2. In pre- and post-expansion phases all aerosol particles were analyzed while during the expansion phase only ice residue was analyzed. Panels (a) and (f) show the time evolution of the temperature and water supersaturation with respect to ice and liquid phase (in dashed, plain, and dotted lines, respectively) in the chamber. For clarity, the temperature scale is not reported on the left of graph (a) but is the same as for (f). Panels (b) and (g) show the PALMS hit rate for positive ion mode (open circles) and for negative ion mode (solid circles) and the OPC raw concentration (solid line). Panels (c) and (h) show the evolution of the particle light scattering from PALMS reported in arbitrary units where larger circles correspond to a higher concentration. Panels (d) and (i) show the evolution of the aerosol composition in positive ion mode expressed as the fraction of particles of a specific class within a given experiment phase. Panels (e) and (j) show the evolution of the aerosol composition in negative ion mode expressed as the fraction of particles of a specific class within a given experiment phase. Note that for both experiments in both polarities hematite particles nucleated ice earlier than illite. Hematite+illite aggregates were found in the ice residue and appear to nucleate similar to pure hematite particles. See text for further details.

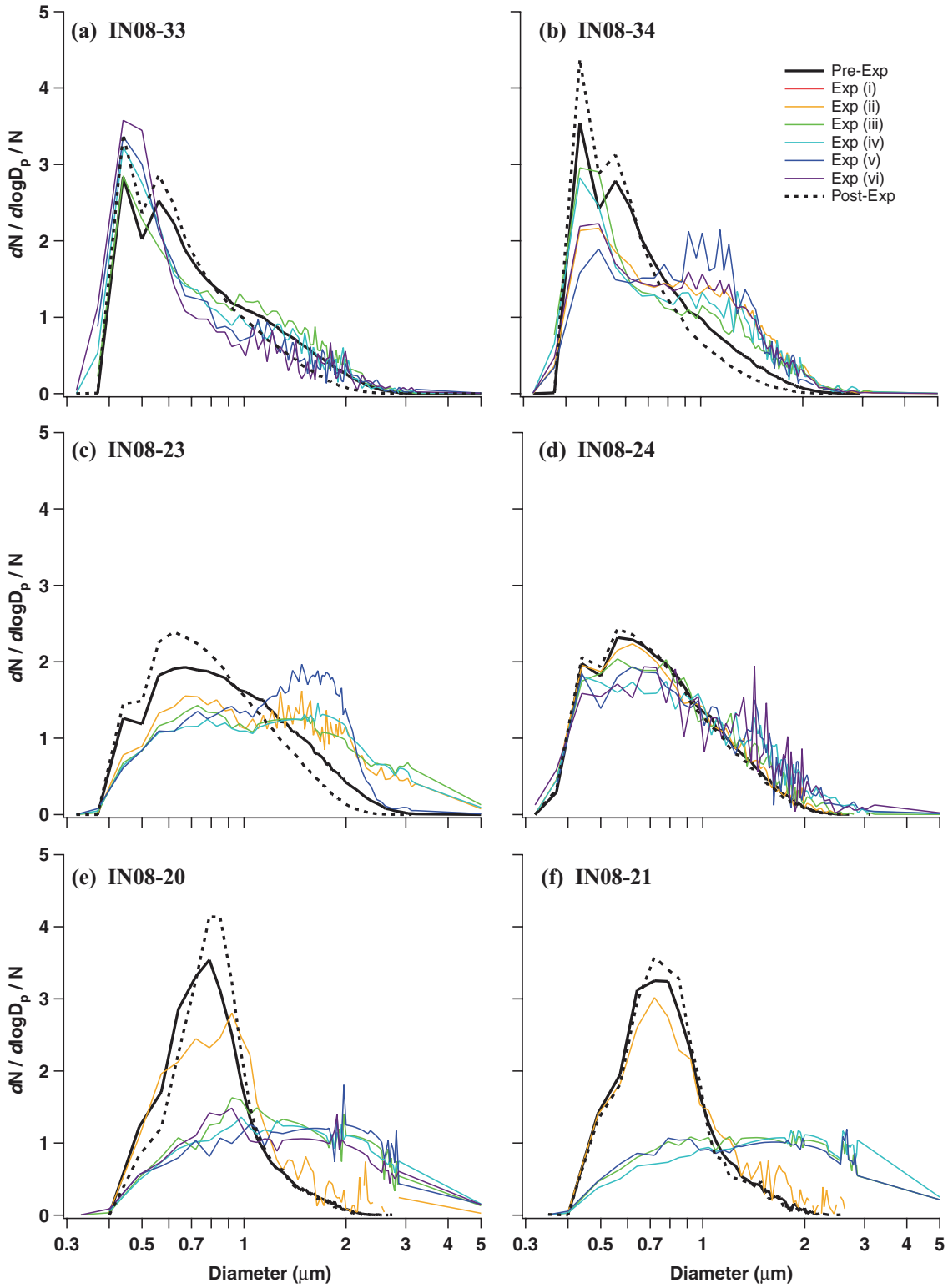

FIG. 7. Normalized OPC size distributions for precursor aerosols (Pre- and Post-Exp) and activated particle residues for time slices Exp (i)–(vi) of six different expansion experiments. The actual size distribution extends below the lower OPC size detection limit for the mineral dust expansions: 33, 34, 23, and 24. The hematite/illite mixture is treated as mineral dust for sizing purposes, and hematite particles within this mixture are oversized by a factor of ~1.6. The PCVI transmitted some interstitial aerosol during expansion 23, time periods (iv) and (v). Calibration glass sphere contamination was removed from distributions in expansions 23, 20, and 21.

fraction of the background particles within the AIDA chamber are effective ice nuclei. This is discussed further in subsequent sections.

Hematite–Illite

Experiments IN08-33 and -34 were conducted with an aerosol consisting of an external mixture of illite and hematite. Both of these mineral dusts are known to be effective heterogeneous ice nuclei when compared to typical atmospheric particles although their relative effectiveness (i.e., which will nucleate ice at a lower saturation and/or higher temperature) was not known *a priori*. Both mineral dusts are differentiable with single particle mass spectrometry (Figure 4).

These and all other experiments discussed below were conducted by first evacuating the chamber and refilling it with particle-free synthetic air. As described in the last section, this included a low number density of chemically distinct background particles. The chamber was cooled to the starting experimental temperature. The pressure was then dropped by pumping air (and aerosol) from the chamber to create a quasi-adiabatic expansion which resulted in a temperature decrease and corresponding saturation increase (Figure 6, panels a and f). The term quasi- is used here because this is not a perfect adiabatic expansion since there is some mixing in the chamber and heat transfer from the walls. At the beginning of the trajectory conditions were always below those required for ice formation by the test aerosol (i.e., the saturation too low and/or the temperature too high). Without ice crystals there should have been no particles with sufficient inertia to pass the PCVI (Figure 7, panels a and b) and no ice residue available for analysis at PALMS (Figure 6, panels b and g). In practice, the fraction of unactivated particles not inertially separated by the PCVI was less than 5×10^{-4}. In a few instances the unactivated particle "leak" rate was higher due to inadequate counterflow (see Figure 7 for one example). Such particles are otherwise eliminated from these analyses. As conditions reached those required for nucleation ice crystals were formed and grew to sufficient size to pass the PCVI and be analyzed. As the experiment progressed the crystal number density increased as the trajectory moved toward higher saturations and lower temperatures. Thus, the most effective ice nuclei were sampled at the beginning of the experiment (e.g., Exp(ii, iii) of IN08-33) while less and less effective ice nuclei entered the ice-phase later and later in the experiment. Eventually, a maximum saturation was reached at which point the ice crystal number density also reached a maximum value. After this point, gravitational settling and evaporation reduced the ice number density. It is important to note that while some limited amount of ice nucleation may have continued to take place after the maximum, the majority of the crystals were formed during the period of increasing saturation. Thus the experimental temperature and saturation at this point were not necessarily related to those that triggered ice nucleation.

It should be noted that in some experiments particles acquired liquid water and acted as cloud condensation nuclei (CCN). Since the PCVI did not discriminate based on phase the droplets were admitted at the same time as ice crystals. The presence of droplets is noted where applicable. One example is some CCN activation early in IN08-34. Droplet activation during these expansions was short (less than 1 min) due to the Bergeron-Findeisen process. These periods are eliminated from this data set using the AIDA facility cloud probes or are otherwise mentioned here.

Figure 6, panels c and h, show the scatter height from the trigger laser for detected particles as a function of experimental time period. Larger circles denote a higher concentration of particles. As previously mentioned, scatter height is an indication of geometric size that is not subject to pressure effects. The initial size distributions of illite and hematite particles are shown in Table 1; illite had a mode size of 0.8 micrometers diameter whereas hematite had a mode size of 0.5. There is an indication that some large particles or aggregates nucleated ice early in these experiments (i.e., Exp(ii) and (iii) of IN08-33) but the data do not allow for quantification. The hematite and illite OPC size distributions overlapped so that the individual components were difficult to optically distinguish when mixed. However, the hematite aerosol had a narrow size distribution with little population above 0.75 μm, whereas illite extended to sizes >1.75 μm. Ice residue was shifted to larger sizes relative to pre- and post-expansion distributions, particularly for IN08-34. Pumping speed was higher for IN08-34, resulting in a sharper onset of ice formation and higher crystal concentrations. The higher crystal surface area in IN08-34 may suggest that large ice residue is the result of scavenging. Size effects were more clear in experiments described in the next sections.

In both experiments hematite was the more effective ice nucleus. Up to 60% of the ice crystals contained hematite whereas less than 40% of the test aerosol was hematite. There is statistical significance to this observation given that $\sim$500 spectra were acquired before, during, and after each of these expansions. The standard error in these cases corresponds to $<3\%$. Further, hematite had the smaller mode size and would have been expected to form an even lower proportion of the ice residue should surface area solely contributing to the efficiency of ice nucleation.

Aggregates of hematite and illite occurred in approximately 12% of the first pre-expansion spectra, indicating that illite-hematite aggregates were present before expansion. In addition, illite-hematite aggregates were enriched in the ice phase (35%) and post-expansion (20%). We can not determine if this is a result of an increased ice nucleation potential for the aggregates although this is likely given that they would have contained one of the better ice nuclei (hematite) and had higher surface area, on average, than a single particle. It should be mentioned that the larger size of aggregates could have helped facilitate their passage through the PCVI. The higher concentration of aggregates in the post-expansion phase suggests that some ice-phase scavenging also occurs during the expansion. This led to more abundant aggregates for the next cycle. Due to the uncertain

processes of gravitational settling—which occurs throughout an expansion and is thus enhanced for the most effective ice nuclei—and removal of particles during pumping we are not able to quantify these processes.

Arizona Test Dust

Experiments IN08-23 and -24 were conducted in the same manner as described for the illite and hematite experiments in the last section (Figure 7c, d and Figure 8). Instead of a two-component external mixture a single aerosol, Arizona test dust, was input to the AIDA chamber. The purpose of these experiments was to test the ice nucleation properties within a mineral dust type. Arizona test dust is a complex mixture of materials. ATD is prepared from a naturally occurring desert sand. The sand is jet milled to reduce the particle size and air classification is used to produce a desired size range. The sample used in this study has the following weight oxide composition: SiO_2 (57.4 %), Al_2O_3 % (13.8 %), CaO (4.3 %), FeO (4.0 %), K_2O (3.8 %), MgO (2.9 %), Na_2O (2.7 %) for a particle size distribution ranging from 50 nm to 2 μm with a mode at 300–400 nm (Möhler et al. 2006).

Both expansions were initiated at -19°C. Once water saturation was achieved, all ATD aerosol activated to form droplets of $\sim$3–5 μm diameter. A fraction of these droplets then froze. The droplet mode was larger and more concentrated for the second expansion although chamber conditions were nearly identical for the two expansions. This may reflect cloud processing during the first expansion.

One feature of these experiments in both the PALMS (Figure 8c, k) and OPC (Figure 7c, d) data is that particles with large light scattering nucleated ice first. OPC distributions show a predominance of large ice residue throughout IN08-23, and a distinct change in the aerosol distribution before and after the expansion. For PALMS, in the case of IN08-23 some signals from the ice residue were larger than the largest pre-expansion signals. This has several possible interpretations. First, since only several hundred spectra were collected in each polarity in the pre-expansion phase it is possible that there was a small fraction of particles of much larger size that were not measured. Second, it is possible these large signals are due to ice-phase scavenging during the expansion. Independent of compositional effects the high surface area of large particles and/or aggregates would favor their nucleation earlier in the expansion than smaller particles. It is unlikely that the large size is due to some amount of residual ice or liquid water because H_2O and cluster ions were not observed in the spectra. In the case of IN08-24 larger residual particles were observed early in the expansion but not with signals as large as in the previous expansion. The OPC data support this: while there is a slight increase in larger ice residue expansion IN08-24 does not show as significant a shift to large sizes. This favors the theory that there was a small amount of large particles at the beginning of the day's experiments which were then lost to gravitational settling during the first expansion and therefore unavailable to nucleate ice in the second.

In both experiments particles with an ATD signature were found in the majority of all ice residues. The initial ice residue in the expansions favored the particles with little or no sulfate and nitrate (i.e., bare mineral dust) whereas the latter species were common toward the end of the expansion. This observation also has several possible explanations. First, sulfate and nitrate were shown to be trace components of the original aerosol. Initial ice nucleation favored the bare dust, which is consistent with observations that surface coatings deactivate ice nucleation by shifting from a deposition to an immersion mode (Pruppacher and Klett 1997). Later in the expansion the coated particles then became active. Further, gravitational settling of the bare particles which nucleated ice early and thus grew to larger crystals resulted in an enrichment of coated particles after the expansion. Alternatively, the increase in sulfate and nitrate could also be attributed to gas-phase scavenging by the ice crystals which was left on the particle after water was evaporated in the PCVI. Neither process can be ruled out and it is possible both played a role in these observations.

Another feature of the ATD experiments was the behavior of the trace mineral species. Li, Rb, Sr, and Ba were found in the pre- and post-expansion particles but were all enriched, except for Li, in the ice residue early in the expansion (Figure 8f, n). What is not certain is if these species played a direct role in the nucleation process or if they are more apparent on particles without a surface coating (i.e., those that formed ice at the beginning of the expansions). This is discussed in subsequent sections. A similar behavior was observed for particles that did not exhibit iron ions. Conversely, carbonaceous material and chlorine were observed on approximately 80% and 30% of the particles, respectively, during the pre- and post-expansion phases for both experiments (Figure 8g, o) but were depleted in the ice residue. Again, it is not clear if these species deactivated the ice nuclei as has been suggested for sulfate and nitrate. This behavior was also observed for particles that only exhibited sulfate, nitrate, and organic features and those with a negative polarity mass 42 peak (CNO^- or $CO_2H_2^-$).

Sulfuric Acid

Experiments IN08-20 and -21 were similar to the ATD experiments in that only a single aerosol, in this case sulfuric acid, was input to the AIDA chamber. Unlike ATD, sulfuric acid particles only undergo homogeneous freezing (i.e., they do not act as heterogeneous IN). Although homogeneous freezing is understood to be a volume-dependant process that is a function of the water activity of the aerosol system (Koop et al. 2000) almost all pre-existing sulfuric acid aerosol activated to form droplets. Thus the original aerosol size was not necessarily related to the size of the droplet which froze and, in turn, the ice residue size.

The results of these experiments, presented in Figures 7 and 9, were more complicated than expected. First, both expansions exhibited a mode of particles large enough to pass through the PCVI before homogeneous freezing conditions were reached (Figure 7e, f and Figure 9b, g) and a part this aerosol exhibited

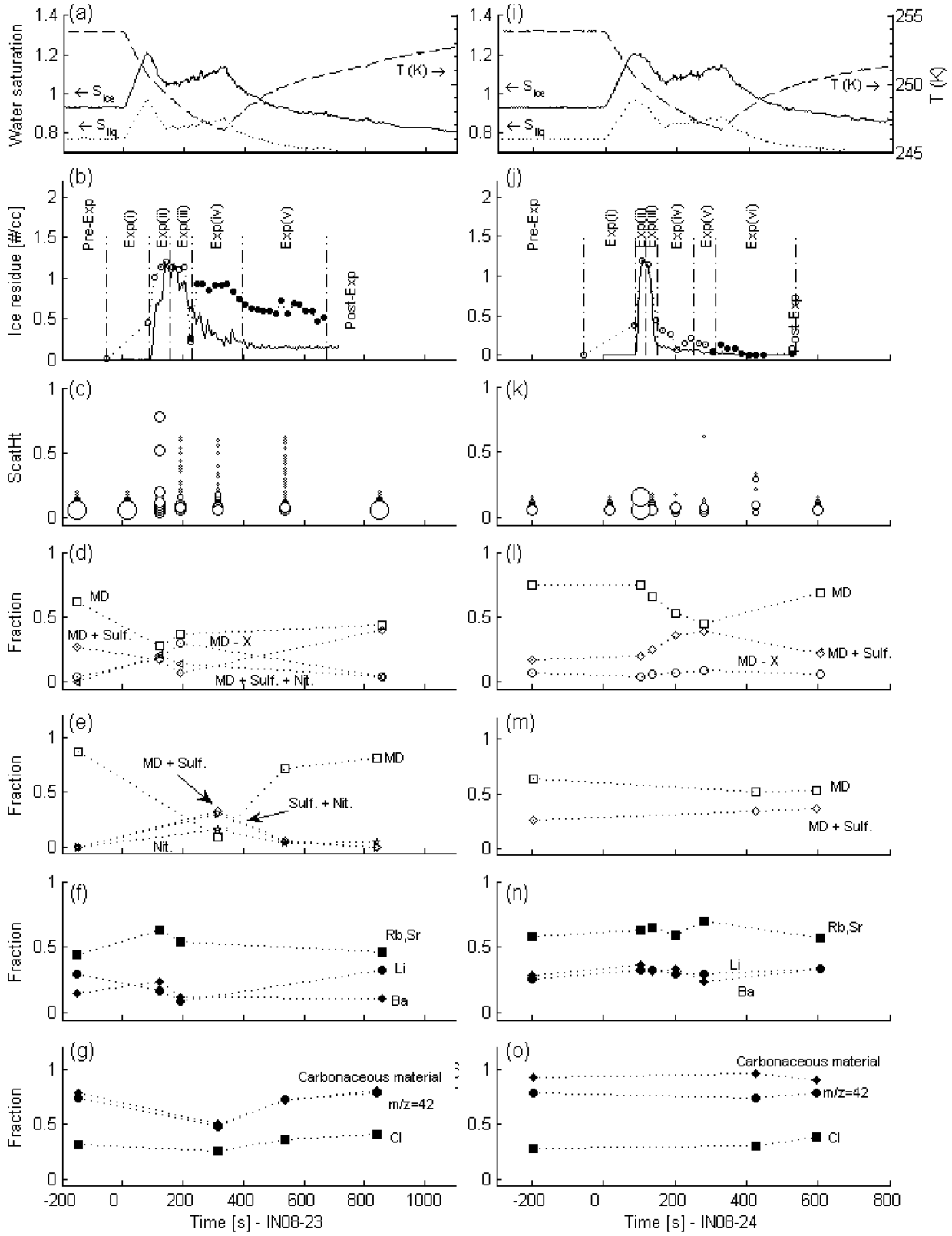

FIG. 8. Data as presented in Figure 6 but for Arizona test dust in expansions IN08-23 (left) and -24 (right). In these expansions panels (f) and (n) show the evolution of trace species in positive ion mode expressed as the proportion of particles containing Li, Rb, Sr, and Ba for each experiment phase. Panels (g) and (o) show the evolution of the proportion of particles containing carbonaceous material, a negative ion with m/z = 42, and chlorine for each experiment phase. Note that uncontaminated ATD nucleated ice earlier than particles which were contaminated with sulfate and/or organics. See text for further details.

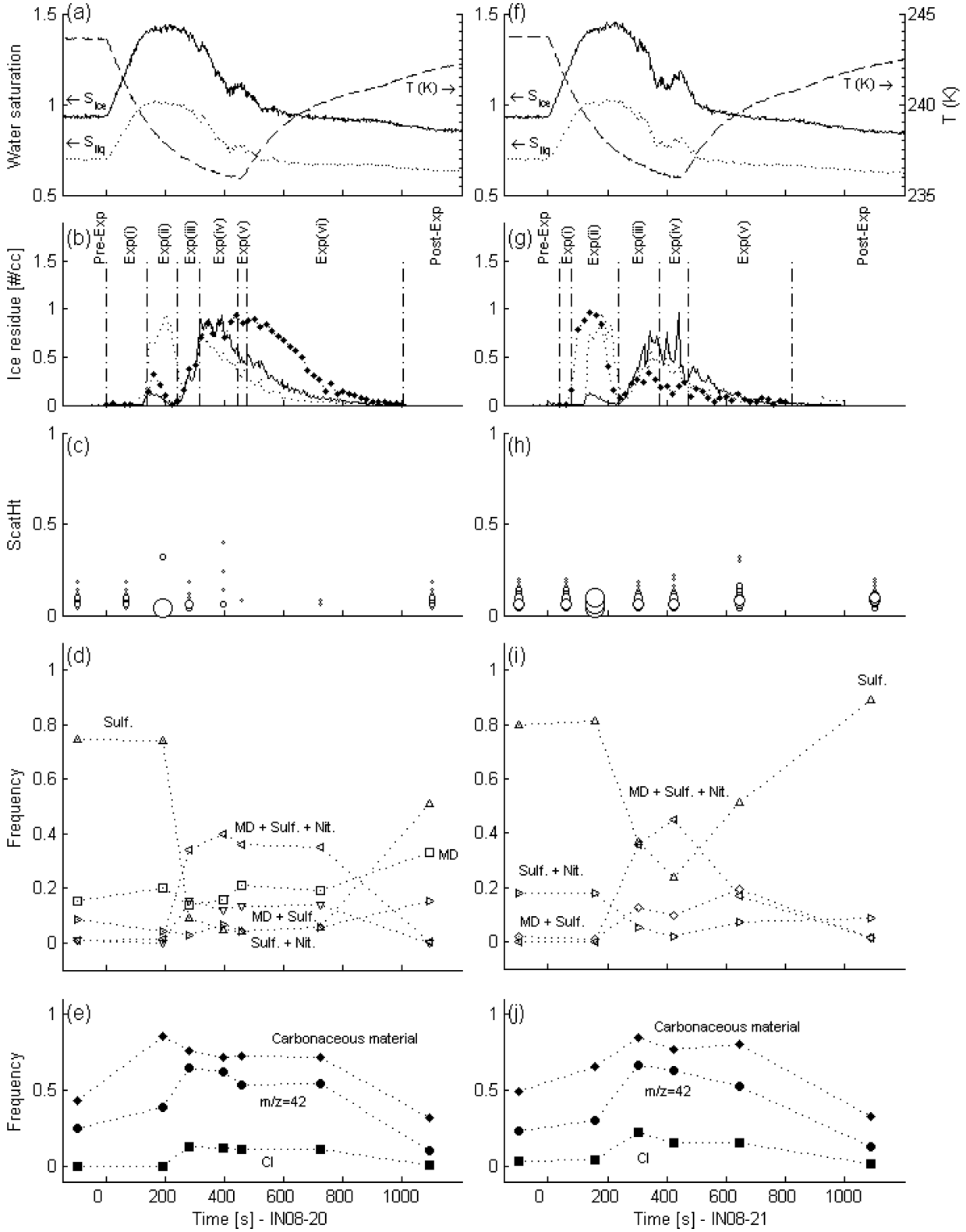

FIG. 9. Data as presented in Figures 6 and 8 but for sulfuric acid test aerosols in expansions IN08-20 (left) and -21 (right). The initial large mode which appeared and then disappeared during each expansion is due to droplet formation and not ice nucleation. In both experiments there was a small heterogeneous freezing mode composed of particles which contained mineral and/or metallic particles although these were not intentionally added to the chamber. Homogeneous freezing is only responsible for the final mode. For clarity the CPC concentration has been scaled by 0.05 and 0.07 in panels (b) and (g) and the OPC by 0.15 and 0.13 in panels (b) and (g), respectively. See text for further details.

a larger light scattering than the average at pre-expansion (Figure 9c, h). The particles in this mode were sulfuric acid, which should not have nucleated ice at these conditions. As presented in Table 4, for both expansions the relative variation of the measured residue concentration at PALMS, OPC, and CPC, scaled for clarity, suggests that the residue was largely smaller than the OPC detection limit (∼300 nm diameter) but at least some were larger than for PALMS (200 nm diameter). For experiment IN08-21 residue concentration, measured from PALMS and CPC, varied similarly. This pre-homogeneous freezing residue is, therefore, from sulfuric acid activation into droplets larger than the cutoff size of the PCVI. This provided a fortuitous source of data. Independent and accurate information about the droplet number and size distribution is available from AIDA facility Welas measurements and FTIR retrievals and this was used to estimate the PCVI cutpoints (Figure 3). The early expansion mode is thus attributed to large aqueous particles, not ice crystals.

Another unexpected result was that approximately 20% of the pre-expansion spectra for both experiments contained features attributed to mineral dust, metals, and nitrates. Further, the mineral and metal-containing particles were observed to nucleate ice in advance of the homogeneous freezing threshold (i.e., they acted as IN). As the expansion proceeded, the proportion of sulfuric acid ice residue increased. This behavior is apparent in both expansions but is more clear in IN08-21. Note that the lower PALMS size limit of 200 nm diameter means that this result is limited to that residue larger than this size. If significant ice nucleation occurred on sulfuric acid particles below this size, and no background aerosol fell below this size, then this ratio is an upper limit.

Carbonaceous material and chlorine containing particles were not observed in high concentration either before or after the expansions. Carbonaceous material was anti-correlated with the pure sulfuric acid particles for the homogeneous freezing mode. Sulfuric acid particle of the early liquid mode were found to contain some carbonaceous material. Chlorine was correlated with mineral dust particle containing sulfates and nitrates (Figure 10a). It remains unclear if this was an aerosol contaminate from production or resulted from gas-phase uptake. Nitrate was observed on the aerosol in the pre-expansion phase and in ice residue as the expansion proceeded (Figure 10b). Nitrates associated with mineral dust and sulfate particles were enriched while

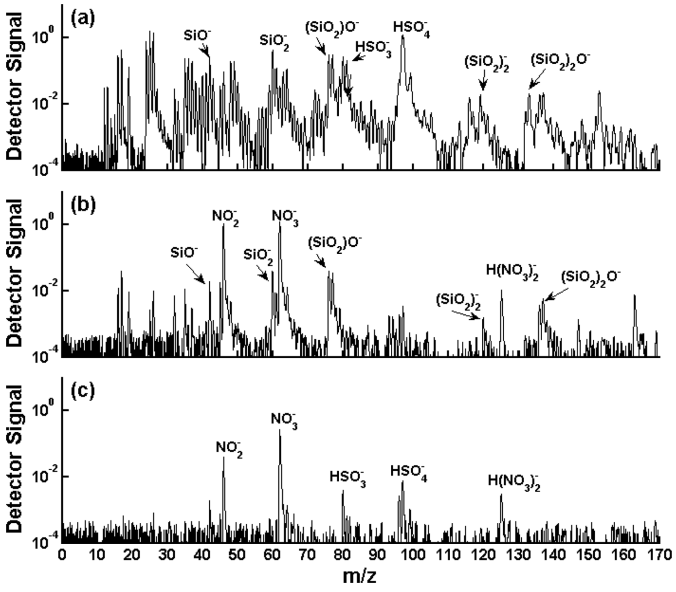

FIG. 10. Examples of particle processing during expansion IN08-20. Particles were analyzed which contained silicates, sulfates, and other miscellaneous species (organics, nitrates, etc.) (a), nitrates and silicates (b), and nitrates and sulfates (c). Only sulfuric acid particles were intentionally input to the chamber before the expansion.

those internally mixed with nitrate and sulfates were depleted in ice residue (Exp(iii, iv, v)). After the expansion, nitrate was not apparent on the mineral and metal-containing particles although it was internally mixed with sulfuric acid aerosol in approximately 10–15% of the spectra (Figure 10c). This behavior is consistent with gas-phase uptake by ice during the expansion. It is not clear why the nitrate left the mineral and metal-containing aerosol rapidly but remained in the sulfuric acid for a longer period.

In summary, the sulfuric acid expansions were more complex than expected. Both expansions exhibited a period of droplet activation that produced particles of sufficient inertia to pass the PCVI. Both expansions showed evidence of heterogeneous freezing by background particles, including mineral dust aerosol which was not adequately removed from the chamber before the experiment. The OPC distributions clearly show two distinct residues for the droplet and ice phases. In agreement with

TABLE 4
Size fractions of activated particle residue

Exp. ID	CPC particles cm^{-3}	OPC[a] particles cm^{-3}	Percent of particles[b] >0.7μm	>1 μm	>2 μm	>3μm
IN08 Pre-20	33.4	17.8	66.4	21.1	0.3	<0.1
IN08 Pre-21	27.8	12.4	62.3	20.0	0.3	<0.1

[a]OPC concentrations are not corrected for wall loss or size biases. [b]Relative to total OPC concentration.

the PALMS composition data, the droplet phase resembles sulfuric acid aerosol, whereas the ice residue was much larger, extending above 3 μm diameter. This result illustrates the complex processes during even simple experiments within the AIDA chamber.

DISCUSSION

Particle Processing

Uptake of gas-phase species was observed in many experiments. The presence of nitrates, carbonaceous material, chlorine and sulfates on ice residue suggests uptake of H_2SO_4, HCl, HNO_3, and organic material was common (e.g., Figures 8e and 9d, e, i, j). Experiments with ATD showed that during the expansion phase sulfates and nitrates were present on some of the mineral dust. For example, in experiment IN08-24 approximately 40% of ice residue consisted of mineral dust associated with sulfates. The "coated" ATD particles were not as effective ice nuclei as their bare counterparts. Uptake of hydrochloric and nitric acid on ice is reported at low temperature in the review of Huthwelker et al. (2006) and the uptake of sulfuric acid on ice can also be expected due to its low vapor pressure. Studies reported in Usher et al. (2003) illustrate the uptake of nitric acid and organics on mineral dusts. Murphy and Thomson (2000) showed evidence of chlorine uptake on mineral particles at low temperature. Uptake of nitric acid on ATD specifically is reported by Vlasenko et al. (2006). Uptake of these species onto dust can occur either directly onto mineral particles or onto ice once it has nucleated. The addition of condensable material onto mineral dust may then affect the nucleating properties during subsequent expansions. These mechanisms can be better differentiated in future measurements if both the unactivated particles and the ice phase were simultaneously monitored.

The origin of the contaminants remains unclear. Sulfuric and nitric acid and carbonaceous material had been used as aerosols and aerosol components during previous experiments in the AIDA chamber. All three substances could have deposited to the walls and then transferred via the gas-phase during pre- and expansion phases. The alternative explanation is that this material was input to the chamber before each expansion as a contaminant in the aerosol production process, as is known to be the case for chlorine with hematite.

Particle aggregation was also suggested in several experiments, either during aerosol production or during the experiment. In expansions IN08-33 and -34 up to 35% of the particles were identified as aggregates of hematite and illite. Data during both experiments showed 15% of particles were aggregates even before ice nucleation began. Once the expansion terminated, the proportion of such aggregates returned to less than 20%. This observation suggests that the ice nucleation step also induced aggregation of particles and this is further discussed in the next paragraph. Expansions may therefore alter the mixing state of the test aerosol by converting an external mixture to an internal one. Aggregation can not be discerned in the case of a single-component system since there is no chemical alteration. Some experiments did show insignificant aggregation, as would be expected given the short residence time of the aerosol in the chamber (hours) and the low particle concentrations. Of two experiments on ATD and sulfuric acid external mixtures (IN08-22 and IN08-25, conducted in IN08 but not described in detail here) only one showed the presence of ATD particles with sulfates and then only corresponding to about 5% of the aerosol. What remains unknown is the fraction of collisions that result in sticking, how the process changes when two aerosols or an ice crystal and aerosol participate, and differences dependant on aerosol chemistry. Further experiments are required to quantify these processes.

For many of the experiments the residue distribution shifted toward larger sizes as the expansion progressed (e.g., Figure 6). One explanation is that large ice particles coagulated with interstitial aerosol, leaving an aggregate once the ice evaporated. PALMS results from the hematite/illite external mixture experiments show that some amount of coagulation occurred. Another possibility is that the largest aerosols in the distribution preferentially nucleated. During the expansions, a substantial fraction of the activated particles impact the chamber walls and are removed from the gas phase. Post-expansion aerosol distributions are often depleted in large sizes relative to pre-expansion, suggesting that larger aerosol indeed preferentially nucleated and were subsequently removed. The large particle depletion was often less apparent for subsequent identical expansions. In order to determine if residues might also have contained enough unevaporated water to increase their diameter two tests were performed. First, size distributions did not change when the sample line temperature was occasionally ramped from 40 to 70°C. Second, no obvious increase in H_2O-related ions was found in the PALMS data for larger residue. Together, this indicates that unevaporated water was not a large fraction of the particle mass during analysis. PALMS results show condensation of contaminant gases on ice crystals during the expansion. However, the condensed gas mass would have to be greater than the original aerosol particle in order to explain the shift in diameter observed during some expansions.

PALMS Analysis Uncertainties

It should be noted that the PALMS analysis method is not without biases. Some of these have been mentioned previously in the text but are reiterated here. Foremost, single particle laser ablation instruments are subject to "matrix effects." Specifically, the phase, composition, water content, and other properties of the aerosol directly impacts the quality of the spectra produced (Johnston 2000). Furthermore, an aerosol must be of a specific size in order to pass through the detection and desorption and ionization laser beams at the correct time to be analyzed. In the case of the PALMS instrument particles with a vacuum aerodynamic diameter less than 200 nm or greater than ~2000 nm are detected progressively less frequently due to their high or low

velocity at the exit of the aerodynamic lens, respectively (Cziczo et al. 2006).

These issues are relevant to the present study. For the hematite–illite and ATD experiments many ice residues, up to 75%, did not produce a mass spectrum. This is likely related to large particles or aggregates that were detected by light scattering but were not present in the desorption and ionization region at the required time. For the experiments on ATD the detected fraction of particles without a coating of sulfates, nitrates, and/or organics should be considered a lower limit. This is because the production of mass spectra from mineral dust is more difficult than for other substances due to its material properties (Gallavardin et al. 2007). Surface coatings enhance particle detection so that the reported proportion of coated particles may be relatively overestimated. ATD particles containing Rb, Sr, and Ba, whose ionization threshold is low, may likewise be relatively overestimated.

The effect of water processing of particles in laser ablation mass spectrometry is not fully understood. The presence of water can "quench" the signal of minor elements (Neubauer et al. 1998). On the other hand, deliquescence followed by drying can enrich the particle surface in minor components (Ge et al. 1996). Gustafsson et al. 2005 report particle growth factor of up to 1.08 for ATD particles (i.e., a diameter increase of 8% due to water uptake). This may offer an explanation as to the enhancement of Rb, Sr, and Ba in the ice residues if they were present in a soluble state and partitioned to the surface.

CONCLUSION

The addition of the PCVI-PALMS system to the suite of instruments available at the AIDA chamber is reported here. The AIDA chamber was used to generate ice crystals by heterogeneous nucleation from external mixtures of illite, hematite, and ATD. Sulfuric acid, which only nucleates homogeneously, was used in some experiments for comparison. Ice crystals were separated from the interstitial aerosol and sent to the PALMS instrument and an OPC and/or CPC for characterization. The PALMS instrument sized and chemically analyzed the ice residue at the single particle level. Since PALMS operates on a rapid (7 Hz) and on-line basis, it was possible to follow changes in particle properties over the course of an ice cloud expansion experiment. In this manner, the ice nucleation properties of each particle type could be related to their respective size and composition. It was found that bare mineral dusts particles were more effective ice nuclei than those coated with sulfates or nitrates. Hematite nucleated ice more effectively than illite for a given particle size. The presence of trace elements such as rubidium, strontium, and barium were more frequently detected in the ice residue and this suggests they could have a role in atmospheric ice nucleation. The PALMS data analysis also demonstrated the occurrence of particle processing during expansions. Aggregation was found to take place when crystals were present, indicative of particle-phase scavenging by ice. Coagulation in the absence of ice crystals between experiments—with a timescale of hours—was also observed. Uptake of residual trace gases and/or material deposited on the chamber walls from previous experiments—such as sulfuric and nitric acid—was also observed. Contamination of the test aerosol with organics, which was not used in recent previous experiments, was common.

PALMS analyses not only showed the presence of these contaminants but this also provided a fortuitous source of data with respect to ice nucleation experiments. By differentiating ATD which had acquired a coating of sulfate with bare ATD it was possible to show that the uncoated material acted as a more efficient ice nucleus. This result agrees with previous studies (Pruppacher and Klett 1997). Likewise, background metal oxide particles found to exist within the chamber could act as effective ice nuclei during experiments where only homogeneous freezing nuclei were meant to be present.

This study shows the advantages of adding a single particle mass spectrometer to the suite of instruments available at AIDA. One strength of this technique is in differentiating external mixtures, especially situations where the test aerosol is chemically distinct while the size, shape, and density are not. A second advantage of this technique is to characterize aerosol properties at levels below other available instruments (e.g., low concentration background aerosols and surface contaminants). This suggests that future experiments which take advantage of these previously unavailable capabilities can now be successfully performed.

REFERENCES

Abbatt, J. P. D., Benz, S., Cziczo, D. J., Kanji, Z., Lohmann, U., and Moehler, O. (2006). Solid Ammonium Sulfate Aerosols as Ice Nuclei: A Pathway for Cirrus Cloud Formation, *Science* 313(5794):1770–1173.

Archuleta, C. M., DeMott, P. J., and Kreidenweiss, S. M. (2005). Ice Nucleation By Surrogates for Atmospheric Mineral Dust and Mineral Dust/Sulfate Particles at Cirrus Temperatures, *Atmos. Chem. Phys. Discuss.* 5:3391–3436.

Boulter, J. E., Cziczo, D. J., Middlebrook, A. M., Thomson, D. S., and Murphy, D. M. (2006). Design and Performance of a Pumped Counterflow Virtual Impactor, *Aerosol Sci. Technol.* 40:969–976.

Braham, R. R., and Spyers-Duran, P. (1974). Ice Nucleus Measurements in an Urban Atmosphere, *J. Appl. Meteor.* 13:940–945.

Cantrell, W., and Heymsfield, A. (2005). Production of Ice in Tropospheric Clouds, *Bull. Amer. Meteor. Soc.* 86(6):795–807.

Cross, E. S., Slowik, J. G., Davidovits, P., Allan, J. D., Worsnop, D. R., Jayne, J. T., Lewis, D. K., Canagaratna, M., and Onasch, T. B. (2007). Laboratory and Ambient Particle Density Determinations using Light Scattering in Conjunction with Aerosol Mass Spectrometry, *Aerosol Sci. Technol.* (4):343–359.

Cziczo, D. J., DeMott, P. D., Brock, C., Hudson, P. K., Jesse, B., Kreidenweiss, S. M., Prenni, A. J., Schreiner, J., Thomson, D. S., and Murphy, D. M. (2003). A Method for Single Particle Mass Spectrometry of Ice Nuclei, *Aerosol Sci. Technol.* 37:460–470.

Cziczo, D. J., Thomson, D. S., Thompson, T. L., DeMott, P. D., and Murphy, D. M. (2006). Particle Analysis by Laser Mass Spectrometry (PALMS) Studies of Ice Nuclei and other Low Number Density Particles, *Int. J. Mass Spectrom.* 258:21–29.

DeMott, P. J. (1990). An Exploratory Study of Ice Nucleation by Soot Aerosols, *J. Applied Meteor.* 29:1072–1079.

DeMott, P. J., Chen, Y., Kreidenweis, S. M., Rogers, D. C., and Sherman D. E. (1999). Ice Formation by Black Carbon Particles, *Geophys. Res. Lett.,* 26(16): 2429–2432, doi: 10.1029/1999GL900580.

DeMott, P. J. (2002). Laboratory Studies of Cirrus Cloud Processes, in *Cirrus*, D. K. Lynch, K., Sassen, D. C. Starr, and G. Stephens, eds., Oxford University, New York, pp. 102−135.

DeMott, P. J., Cziczo, D. J., Prenni, A. J., Murphy, D. M., Kreidenweiss, S. M., Thomson, D. S., Borys, R., and Rogers, D. C. (2003). Measurements of the Concentration and Composition of Nuclei for Cirrus Formation, *Proc. Nat. Acad. Sci.* 100(25):14655–14660.

Diehl, K., and Mitra, S. K. (1998). A Laboratory Study of the Effects of a Kerosene-burner Exhaust on Ice Nucleation and the Evaporation Rate of Ice Crystals, *Atmos. Environ.* 32:3145–3151.

Dymarska, M., Murray, B. J., Sun, L. M., Eastwood, M. L., Knopf, D. A., and Bertram, A. K. (2006). Deposition Ice Nucleation on Soot at Temperatures Relevant for the Lower Troposphere, *J. Geophys. Res.* 111 (D4), doi:10.1029/2005JD006627.

Forster, P., Ramaswamy, V., Artaxo, P., Berntsen, T., Betts, R., Fahey, D. W., Haywood, J., Lean, J., Lowe, D. C., Myhre, G., Nganga, J., Prinn, R., Raga, G., Schulz, M., and Van Dorland, R. (2007). Changes in Atmospheric Constituents and in Radiative Forcing, in *Climate Change 2007: The Physical Science Basis. Contribution of Working Group I to the Fourth Assessment Report of the Intergovernmental Panel on Climate Change*, S. Solomon, D. Qin, M. Manning, Z. Chen, M. Marquis, K. B. Averyt, M. Tignor, and H. L. Miller, eds., Cambridge University Press, Cambridge, UK and New York.

Gallavardin, S., Cziczo, D. J., and Lohmann, U. (2007). Analysis and Differentiation of Mineral Dust by Single Particle Laser Mass Spectrometry, *Int. J. Mass. Spectrom.* in review.

Ge, Z., Wexler, A. S., and Johnston, M. V. (1996). Multicomponent Aerosol Crystallization, *J. Colloid Interf. Sci.* 183:68–77.

Georgii, H. W. (1963). Investigations on Deactivation of Inorganic and Organic Freezing-Nuclei, *Z. Agnew. Math. Phys.* 14:503–510.

Gorbunov, B., Baklanov, A., Kakutkina, N., Windsor, H. L., and Toumi, R. (2001). Ice Nucleation on Soot Particles, *J. Aerosol Sci.* 32:199–215.

Gustafsson, R. J., Orlov, A., Badger, C. L., Griffiths, P. T., Cox, R. A., and Lambert, R. M. (2005). A Comprehensive Evaluation of Water Uptake on Atmospherically Relevant Mineral Surfaces: DRIFT Spectroscopy, Thermogravimetric Analysis and Aerosol Growth Measurements, *Atmos. Chem. Phys.* 5:3415–3421.

Huthwelker, T., Ammann, M., and Peter, T. (2006). The Uptake of Acidic Gases on Ice, *Chem. Rev.* 106 (4):1375–1444.

Johnston, M. V. (2000). Sampling and Analysis of Individual Particles by Aerosol Mass Spectrometry, *J. Mass Spectrom.* 35:585–595.

Koop, T., Luo, B. P., Tsias, A., and Peter, T. (2000). Water Activity as the Determinant for Homogeneous Ice Nucleation in Aqueous Solutions, *Nature* 406(6796):611–614.

Liu, P. S. K., Deng, R., Smith, K. A., Williams, L. R., Jayne, J. T., Canagaratna, M. R., Moore, K., Onasch, T. B., Worsnop, D. R., and Deshler, T. (2007). Transmission Efficiency of an Aerodynamic Focusing Lens System: Comparison of Model Calculations and Laboratory Measurements for the Aerodyne Aerosol Mass Spectrometer, *Aerosol Sci. Technol.* 41:721–733.

Möhler, O., Büttner, S., Linke, C., Schnaiter, M., Saathoff, H., Stetzer, O., Wagner, R., Krämer, M., Mangold, A., Ebert, V., and Schurath, U. (2005). Effect of Sulfuric Acid Coating on Heterogeneous Ice Nucleation by Soot Aerosol Particles, *J. Geophys. Res.* 110, D11210, doi:11210.11029/12004JD005169.

Möhler, O., Field, P. R., Connolly, P., Benz, S., Saathoff, H., Schnaiter, M., Wagner, R., Cotton, R., Kraemer, M., Mangold, A., and Heymsfield, A. J. (2006). Efficiency of the Deposition Mode Ice Nucleation on Mineral Dust Particles, *Atmos. Chem. Phys. Discuss.* 6: 3007–3021.

Möhler, O., Linke, C., Saathoff, H., Schnaiter, M., Wagner, R., Mangold, A., Kramer, M., and Schurath, U. (2005). Ice Nucleation on Flame Soot Aerosol of Different Organic Carbon Content, *Meteorologische Zeitschrift,* 14(4):477–484.

Möhler, O., Stetzer, O., Schaefers, S., Linke, C., Schnaiter, M., Tiede, R., Saathoff, H., Kramer, M., Mangold, A., Budz, P., Zink, P., Schreiner, J., Mauersberger, K., Haag, W., Karcher, B., and Schurath, U. (2003). Experimental Investigation of Homogeneous Freezing of Sulphuric Acid Particles in the Aerosol Chamber AIDA , *Atmos. Phys. Chem.* 3:211–223.

Murphy, D. M., and Koop, T. (2005). Review of the Vapour Pressures of Ice and Supercooled Water for Atmospheric Applications, *Q. J. Roy. Meteor. Soc.* 131:1539–1565.

Murphy, D. M., Cziczo, D. J., Hudson, P. K., Schein, M. E., and Thomson, D. S. (2004). Particle Density inferred from Simultaneous Optical and Aerodynamic Diameters Sorted by Composition, *J. Aerosol Sci.* 35(1):135–139.

Murphy, D. M., and Thomson, D. S. (2000). Halogen Ions and NO^+ in the Mass Spectra of Aerosols in the Upper Troposphere and Lower Stratosphere, *Geophys. Res. Lett.* 27(19):3217–3220.

Moffet, R. C., and Prather, K. A. (2005). Extending ATOFMS Measurements to Include Refractive Index and Density, *Anal. Chem.* 77(20):6535–6541.

Neubauer K. R., Johnston M. V., and Wexler A. S. (1998). Humidity Effects on the Mass Spectra of Single Aerosol Particles, *Atmos. Environ.* 32(14–15):2521–2529.

Prather, A. K., Nordmeyer, T., and Salt, K. (1994). Real-Time Characterization of Individual Aerosol Particles using Time-of-Flight Mass Spectrometry, *Anal. Chem.* 66:1403–1407.

Pruppacher, H. R., and Klett, J. D. (1997). *Microphysics of Clouds and Precipitation,* 2nd Edition. Kluwer Academic Publishers, Netherlands.

Seifert, M., Tiede, R., Schnaiter, M., Linke, C., Möhler, O., Schurath, U., and Ström, J. (2004), Operation and Performance of a Differential Mobility Particle Sizer and a TSI 3010 Condensation Particle Counter at Stratospheric Temperatures and Pressures, *J. Aerosol Sci.* 35:981–993.

Twomey, S. (1974). Pollution and Planetary Albedo, *Atmos. Environ.* 8(12):1251–1256.

Usher, C. R., Michel, A. E., and Grassian, V. H. (2003). Reactions on Mineral Dust, *Chem. Rev.* 103:4883–4939.

Vali, G., Rogers, D. C., Gordon, D., Saunders, C. P. R., Reischel, M., and Black, R. (1978). Aerosol and Nucleation Research. In Support of NASA Cloud Physics Experiments in Space, *NASA Final Report,* 1–86.

Vlasenko, A., Sjogren, S., Weingartner, E., Stemmler, K., Gaggeler, H. W., and Ammann, M. (2006). Effect of Humidity on Nitric Acid Uptake to Mineral Dust Aerosol Particles, *Atmos. Chem. Phys.* 6:2147–2160.

Wilson, J. C., and Liu, B. Y. (1980). Aerodynamic Particle Size Measurement by Laser-Doppler Velocimetry, *J. Aerosol Sci.* 11:139–150.

Zelenyuk, A., and Imre, D. (2005). Single Particle Laser Ablation Time-of-Flight Mass Spectrometer: An Introduction to SPLAT, *Aerosol Sci. Technol.* 39:1–15.

Zhang, X., Smith, K. A., Worsnop, D. R., Jimenez, J. L., Jayne, J. T., Kolb, C. E., Morris, J., and Davidovits, P. (2004). Numerical Characterization of Particle Beam Collimation: Part II Integrated Aerodynamic-Lens-Nozzle System, *Aerosol Sci. Technol.* 38:619–638.

Zobrist, B., Marcolli, C., Koop, T., Luo, B. P., Murphy, D. M., Lohmann, U., Zardini, A. A., Krieger, U. K., Corti, T., Cziczo, D. J., Fueglistaler, S., Hudson, P. K., Thomson, D. S., and Peter, T. (2006). Oxalic Acid as a Heterogeneous Ice Nucleus in the Upper Troposphere and its Indirect Aerosol Effect, *Atmos. Chem. Phys.* 6:3115–3129.